energies

MDPI

Article

Efficiency Advantages of the Separated Electric Compound Propulsion System for CNG Hybrid Vehicles

Emiliano Pipitone and Salvatore Caltabellotta *

Department of Engineering, University of Palermo, 90128 Palermo, Italy; emiliano.pipitone@unipa.it
* Correspondence: salvatore.caltabellotta@unipa.it

Abstract: As is widely known, internal combustion engines are not able to complete the expansion process of the gas inside the cylinder, causing theoretical energy losses in the order of 20%. Several systems and methods have been proposed and implemented to recover the unexpanded gas energy, such as turbocharging, which partially exploits this energy to compress the fresh intake charge, or turbo-mechanical and turbo-electrical compounding, where the amount of unexpanded gas energy not used by the compressor is dedicated to propulsion or is transformed into electric energy. In all of these cases, however, maximum efficiency improvements between 4% and 9% have been achieved. In this work, the authors deal with an alternative propulsion system composed of a CNG-fueled spark ignition engine equipped with a turbine-generator specifically dedicated to unexpanded exhaust gas energy recovery and with a separated electrically driven turbocompressor. The system was conceived specifically for hybrid propulsion architectures, with the electric energy produced by the turbine generator being easily storable in the on-board energy storage system and re-usable for vehicle traction. The proposed separated electric turbo-compound system has not been studied in the scientific literature, nor have its benefits ever been analyzed. In this paper, the performances of the analyzed turbo-compound system are evaluated and compared with a traditional reference turbocharged engine from a hybrid application perspective. It is demonstrated that separated electric compounding has great potential, with promising overall efficiency advantages: fuel consumption reductions of up to 15% are estimated for the same power output level.

Keywords: hybrid vehicle; compound engine; CNG spark-ignition engine; exhaust energy recovery

Citation: Pipitone, E.; Caltabellotta, S. Efficiency Advantages of the Separated Electric Compound Propulsion System for CNG Hybrid Vehicles. *Energies* **2021**, *14*, 8481. https://doi.org/10.3390/en14248481

Academic Editors: Massimo Cardone and Bonaventura Gargiulo

Received: 20 October 2021
Accepted: 29 November 2021
Published: 15 December 2021

1. Introduction

The ever-increasing cost of hydrocarbons and stringent anti-pollution regulations are driving worldwide governments towards innovative mobility solutions capable of guaranteeing fuel economy and respect for the environment. Aiming to limit global warming to below 2 °C [1], governments and nations are encouraging the adoption of adequate measures to strongly reduce the consumption of oil-derived fuels. The most recent data provided by the European Environment Agency (EEA) show that the transport sector is responsible for about 32% of the total CO_2 emissions in the European Union [2]. In September 2020, the European Commission presented the ambitious proposal to cut greenhouse gas emissions by 55% by 2030. This goal represents the first step towards the wider project that aims to make Europe the first climate-neutral continent by 2050 (European Green Deal) [3].

Among the most interesting and short-term solutions, hybrid electric vehicles (HEVs) certainly represent a valid alternative compared to traditional internal combustion engine vehicles (ICEVs), given the significant fuel savings achieved, especially in urban areas; although good technological levels have already been reached, their development is relatively recent, which is why there is still plenty of room for improvement. In a hybrid thermal-electric architecture, a possible development area is represented undoubtedly by the internal combustion engine, which produces the energy necessary for vehicle trac-

tion and battery charging; a significant increase in the engine efficiency may produce considerable improvements in the efficiency of the entire propulsion system.

As is well-known, internal combustion engines based on Otto or diesel cycles cannot complete the expansion process of the gas inside the cylinder, thus losing a significant proportion of the energy content, in the order of 20% of the total energy content (represented by the two dashed areas in Figure 1).

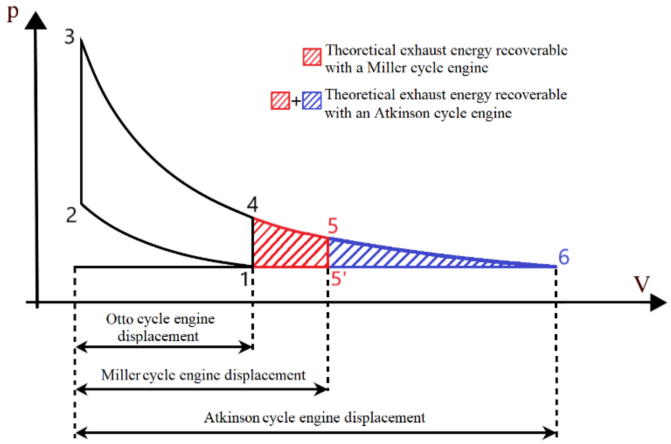

Figure 1. Comparison between the Otto, Miller and Atkinson cycles.

As regards the exploitation of the exhaust gas energy, the best-known system is certainly represented by the exhaust gas turbine used for turbocharging purposes. In this case, the turbine only has the function of providing the mechanical power required by the turbocompressor, thus limiting the amount of recoverable energy from exhaust gas. Several other systems for internal combustion engine exhaust energy recovery can be traced in the scientific literature [4,5]. Many systems focus on recovering the surplus power produced by the turbine and not required by the turbocompressor through the use of an electric generator installed on the turbocharger shaft [6–9] (Figure 2a); another kind of turbo-compound system involves the installation of a second turbine generator downstream of the first turbine in order to recover the exhaust energy not yet exploited (Figure 2b). The first solution (Figure 2a) achieves maximum overall efficiency improvements in the order of 6%, while the second solution (Figure 2b) achieves efficiency improvements of 4% [10,11]. In the naval industry, the second solution (Figure 2b) has been widely adopted, with a second turbine downstream of the first, whose output power is directly added as mechanical power to the propeller shaft. In [12,13], on the other hand, the use of a second turbine in parallel to the first (used for supercharging) was considered, and in both cases the use of both a fixed and a variable geometry turbine was hypothesized. With this type of turbo-compound system, efficiency improvements of up to 9% were observed. Another solution for a better completion of in-cylinder gas expansion is represented by over-expanded cycles, such as Atkinson and Miller cycles [14]. In an Atkinson cycle, the expansion stroke should be extended up to atmospheric pressure [15–17]; this could be achieved through the use of adequate intake valve timing in a properly designed engine. As can be seen from Figure 1 (curve 1-2-3-6-1), the Atkinson cycle allows one to recover both the blue and red area, allowing a theoretical efficiency increase of about 20% compared to the Otto cycle. This would imply, however, an impracticable too large in-cylinder volume, about four times the corresponding volume of the Otto cycle engine. This implies a strong decrease in the engine power density (in the order of −72%).

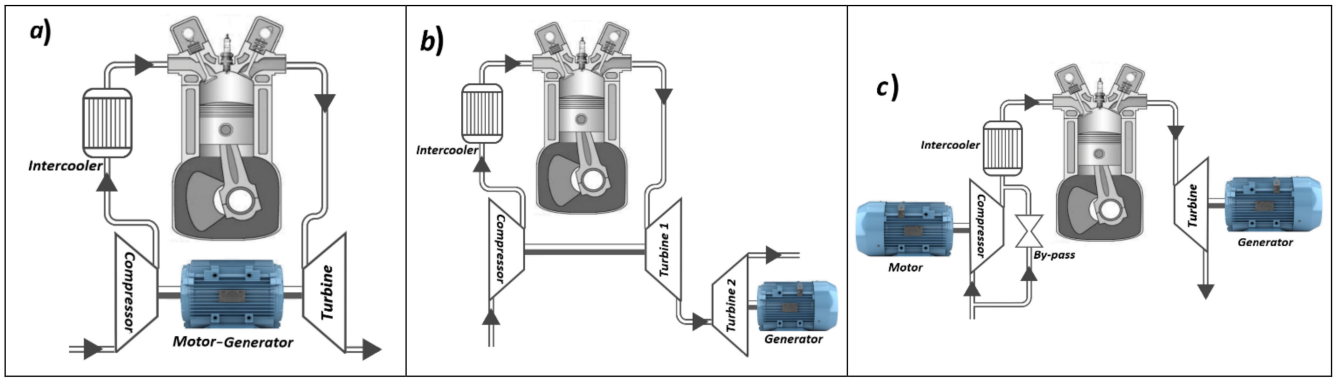

Figure 2. Electric compound systems [4]: (**a**) high-pressure electric compound; (**b**) low-pressure electric compound; (**c**) separated electric compound.

In the Miller cycle, on the other hand, the gas expands down to the pressure p_5 which is significantly higher than the atmospheric pressure [18], thus maintaining plausible in-cylinder volumes. A Miller cycle engine can be practically developed by adopting a high engine geometrical compression ratio (GCR) and early (or late) intake valve closure (IVC). In this way, the compression stroke is limited (avoiding dangerous knocking phenomena), while the expansion stroke can be better exploited [13]: adopting a geometrical compression ratio (GCR) of 14, an 8% theoretical efficiency increment can be obtained with respect to the Otto cycle, to the detriment of the power density, which is reduced by about 25%. A practical application of a Miller cycle engine was made by Toyota in the Prius hybrid vehicle, in which an engine with a geometrical compression ratio of 13 was adopted: through this application, it was possible to obtain an improvement in fuel economy of 8.5% [19]. Although the implementation of a Miller cycle can bring about an improvement in fuel consumption, the resulting power density reduction still represents a crucial drawback which limits its advantages [20].

In this paper, the authors analyze the energetic advantages of a compound system (Figure 2c) composed of an electric supercharged CNG spark ignition engine endowed with a dedicated exhaust gas turbine generator with the aim of recovering the unexpanded exhaust gas energy. The turbine is directly linked to a suitable electric generator, while the compressor is driven by an electric motor. Unlike the compound systems already studied (Figure 2a,b), in this work, the two thermal machines (the compressor and turbine) are disconnected, thus working independently of each other. In turn, each thermal machine is connected to its own electric machine, thus ensuring a more flexible and extensive regulation of the entire system [4]. In the system here proposed, the turbine has the task of recovering as much energy as possible from the exhaust gas, which is converted into electrical energy by the connected electrical generator. The separated electric turbo-compound system is particularly suitable for hybrid propulsion vehicles [21], where the electricity produced by the turbine generator group can be stored in the on-board storage system and then used for vehicle traction. It is important to note that in a hybrid propulsion system, the operating conditions of the thermal engine do not vary as widely and rapidly as in a traditional vehicle; for this reason, the turbine of the compound engine could work in quasi-steady conditions; for this reason, the turbine considered for this application will certainly have a higher efficiency than a traditional turbocharging turbine. Figure 3 shows a possible hybrid vehicle architecture equipped with the electric compound engine proposed in this paper: as is shown, the electric power produced by the turbine generator, together with the power delivered by the motor-generator MG1, is directly stored in the vehicle's storage system, which, in turn, supplies the second electric motor MG2 and the motor-compressor employed for supercharging purposes. It is worth pointing out that the only previous work dealing with the same propulsion system was presented at the 2020 Conference on Sustainable Mobility [22] by the same authors: however, as will be clarified later, many and substantial differences have been introduced in the present paper.

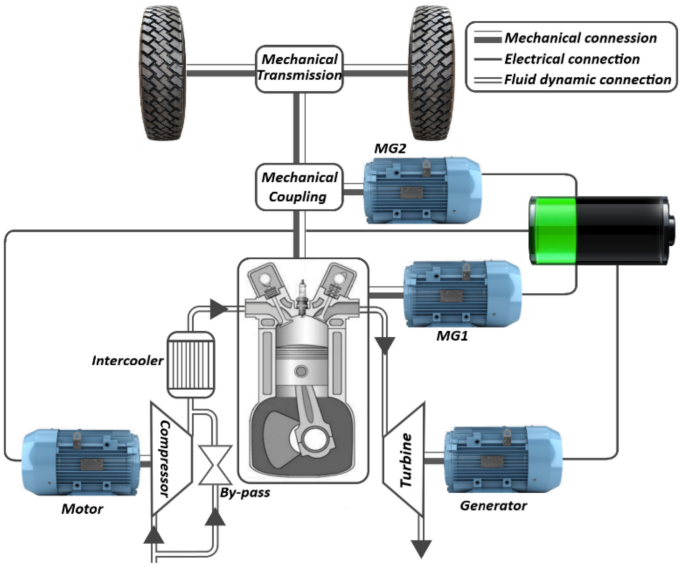

Figure 3. Hybrid propulsion system endowed with the proposed compound engine (MG1 and MG2 = motor-generator units).

In this paper, the steady state performances of the proposed separated electric compound engine are evaluated and compared with the performances of a traditional reference turbocharged engine on an equal power basis, i.e., each propulsion unit was sized to deliver the same continuous maximum power of 73.5 kW (100 HP). Each power unit was also developed starting from the same reference naturally aspirated engine, whose performance evaluation is carried out in the next section. The whole analysis was carried out through a simple modelling approach, mainly based on mass flow and power balance equations, properly accompanied by simplifying assumptions and relations; the theoretical approach was also supported by experimental data derived from the relevant scientific literature or directly measured through experimental tests carried out by the same authors.

2. Baseline Naturally Aspirated Engine

As a first step, the authors developed the steady state performances of the baseline naturally aspirated engine. Starting from the characteristics and the specific performances of this common baseline naturally aspirated engine, the performances of both the separated electric turbo-compound unit and the reference turbocharged engine were obtained. For the development of the baseline naturally aspirated engine model, the authors employed the experimental data of the gasoline VVT spark ignition engine reported in [23]. The system analyzed in the present paper was conceived for a European Type C–Medium hybrid vehicle, which is why the engine performances reported in [23] were remodeled and adapted to a mid-level passenger car engine through a normalization process. For this purpose, the normalized mean piston speed u was employed:

$$u = \frac{u_m}{u_{m,\max}} \; (0 \le u \le 1) \tag{1}$$

As a result, Figures 4 and 5 show the resulting values of:

(1) Brake mean effective pressure (BMEP)
(2) Indicated mean effective pressure (IMEP)
(3) Relative air–fuel ratio (λ)
(4) Volumetric efficiency (λ_V)

as functions of the normalized mean piston speed and for the full load condition (or wide-open throttle, WOT), while Figure 6 shows the BMEP as a function of the manifold absolute pressure (MAP) for a fixed normalized mean piston speed (u = 0.267).

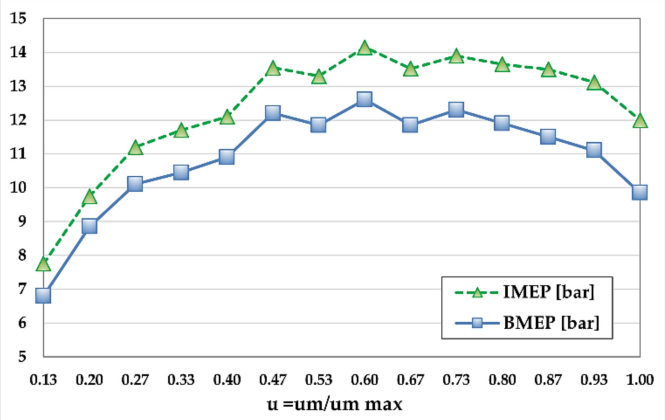

Figure 4. Brake (*BMEP*) and indicated (*IMEP*) mean effective pressure as functions of the normalized mean piston speed u, at full load conditions.

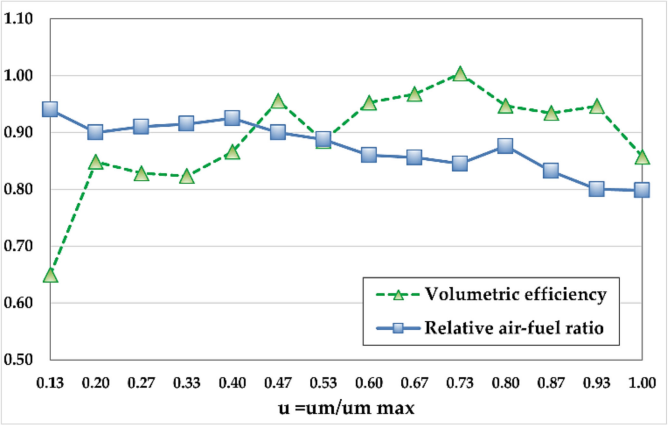

Figure 5. Volumetric efficiency and relative air–fuel ratio as functions of the normalized mean piston speed, at full load conditions.

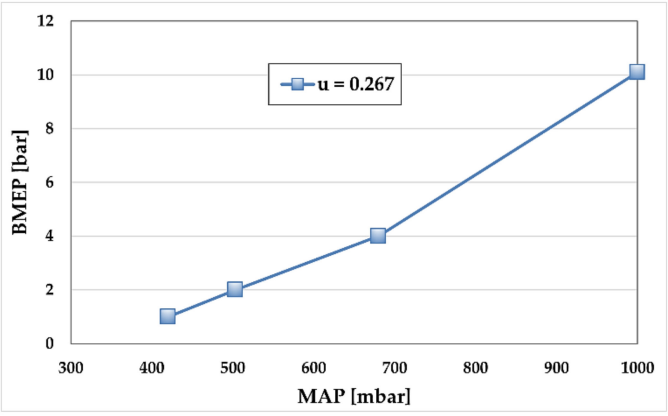

Figure 6. Brake mean effective pressure as a function of manifold absolute pressure (*MAP*) at u = 0.267.

In this work, a modified version of the Chen–Flynn model [24] was adopted for the calculation of the friction mean effective pressure (*FMEP*); in this modified version, the normalized mean piston speed u was adopted instead of engine speed, and the indicated

mean effective pressure IMEP was considered as a pressure load-related variable instead of the maximum in-cylinder pressure:

$$FMEP = A + B \cdot IMEP + C \cdot u + D \cdot u^2 \quad (2)$$

Through a least squares regression process performed on the experimental *BMEP* and *IMEP* data shown in Figures 4 and 6, the values of the four parameters (*A*, *B*, *C* and *D*) were obtained (reported in Table 1).

Table 1. Parameters determined for the Chen–Flynn *FMEP* model.

Parameter	Value
A [bar]	0.630
B [-]	0.0398
C [bar]	−0.00341
D [bar]	0.00366

Once the parameters of the *FMEP* model were determined, the authors adopted the experimental $IMEP_{\text{exp}}$ values shown in Figure 4 for the gasoline-fueled reference engine, while the *BMEP* values were obtained, for each speed and load, by means of the application of the *FMEP* model:

$$BMEP_{gasoline} = IMEP_{\text{exp}} - FMEP \quad (3)$$

As regards the air–fuel ratio, the values shown in Figure 5 were adopted for the full load conditions (i.e., *MAP* = 1 bar), while a stoichiometric mixture (i.e., λ = 1) was assumed for *MAP* values lower than 0.9 bar, as the stoichiometric air-fuel ratio α_{st} = 14.7 for gasoline. For the intermediate operating points with *MAP* between 0.9 and 1 bar, a linear variation of the air–fuel ratio was assumed. The engine indicated efficiency was evaluated starting from the relation between *IMEP* and the engine operating parameters:

$$IMEP = \frac{\delta_A \cdot \lambda_V \cdot LHV}{\lambda \cdot \alpha_{st} + \frac{1}{\delta'}} \cdot \eta_i \quad (4)$$

where *LHV* is the gasoline lower heating value (assumed 43 MJ/kg), η_i is the indicated engine efficiency, δ_A is the air density in the manifold and δ' is the relative fuel density, i.e., the ratio between fuel and air density:

$$\delta' = \delta_F / \delta_A \quad (5)$$

For a multi-point indirect gasoline injection, it is plausible to assume that 40% of the fuel evaporates before entering the cylinder, and thus the average fuel density δ_F is:

$$\delta_F = \delta_{F,V} \cdot 0.4 + \delta_{F,L} \cdot 0.6 \quad (6)$$

where $\delta_{F,L}$ and $\delta_{F,V}$ are the fuel density of the liquid and vapor phase, respectively. The vapor fuel density was evaluated assuming the perfect gas law with a gasoline molecular mass of 100 g/mol [25].

The gross indicated mean effective pressure $IMEP_{g,gasoline}$ of the gasoline-fueled engine was hence calculated on the basis of the $IMEP_{\text{exp}}$ values:

$$IMEP_{g,gasoline} = IMEP_{\text{exp}} + PMEP \quad (7)$$

where the pumping mean effective pressure *PMEP* was simply assumed as:

$$PMEP = MAP - p_{S0} \quad (8)$$

The term p_{S0} represents the in-cylinder pressure during the exhaust stroke of the baseline naturally aspirated engine; here, $p_{0\text{is}}$ considered as 1.10 to account for the pressure drop in the exhaust pipe. The gross indicated efficiency of the gasoline naturally aspirated engine was hence calculated from the gross indicated mean effective pressure:

$$\eta_{i,g,gasoline} = \frac{IMEP_{g,gasoline} \cdot \left(\lambda \cdot \alpha_{st} + \frac{1}{\delta'}\right)}{\delta_A \cdot \lambda_V \cdot LHV} \tag{9}$$

According to the simple approach followed in this analysis, the modeling of the CNG-fueled naturally aspirated engine was performed assuming the same gross indicated efficiency of the gasoline-fueled engine for the same operating points (i.e., the same *MAP* level and engine speed). According to this simplifying assumption, the gross indicated efficiency of the *CNG*-fueled engine $\eta_{ig,CNG}$ was determined starting from the gross indicated efficiency $\eta_{ig,gasoline}$ of the gasoline-fueled engine:

$$\eta_{ig,CNG}(MAP, u) = \eta_{ig,gasoline}(MAP, u) \tag{10}$$

Considering the volumetric efficiency of the engine expressed as the ratio between the mass of the fuel–air mixture m_m $(= m_{air} + m_{fuel})$ actually introduced in the engine at each cycle and the theoretical mass $(V \cdot \delta_m)$:

$$\lambda_V = \frac{m_m}{V \cdot \delta_m} = \frac{m_m}{V \cdot \delta_a} \cdot \frac{\alpha + \frac{1}{\delta'}}{\alpha + 1} \tag{11}$$

another plausible assumption was made on the volumetric efficiency of the *CNG* engine supposedly equal to the gasoline-fueled engine:

$$\lambda_{V,CNG} = \lambda_{V,gasoline} \tag{12}$$

It is worth noting that the assumption made does not imply that the same amount of air enters both *CNG* and gasoline-fueled engine, due to the very different relative density δ' of the two fuels.

The gross indicated mean effective pressure of the *CNG*-fueled naturally aspirated engine was then determined as:

$$IMEP_{g,CNG} = \frac{\delta_A \cdot \lambda_V \cdot LHV_{CNG}}{\lambda \cdot \alpha_{st} + \frac{1}{\delta'}} \cdot \eta_{i,g,CNG} \tag{13}$$

Given the very high knock resistance of natural gas, and adopting the same volumetric compression ratio of the gasoline baseline engine, the *CNG*-powered engine was assumed to run always with a stoichiometric air–fuel ratio (i.e., λ = 1). Considering that rich mixtures cause low combustion (and hence indicated) efficiency, to account for the different mixture strengths adopted with the two fuels, the authors corrected the indicated efficiency of the *CNG*-powered engine, employing as the correction factor the combustion efficiency published in [24] and reported in the diagram of Figure 7, thus obtaining the indicated gross efficiency of the *CNG*-fueled engine operating at a stoichiometric air–fuel ratio:

$$\eta_{i,g,CNG} = \eta_{i,g,gasoline} \frac{\eta_{comb}(\lambda = 1)}{\eta_{comb}(\lambda_{gasoline})} \tag{14}$$

where $\eta_{comb}(\lambda_{gasoline})$ is the combustion efficiency related to the gasoline relative air–fuel ratio λ.

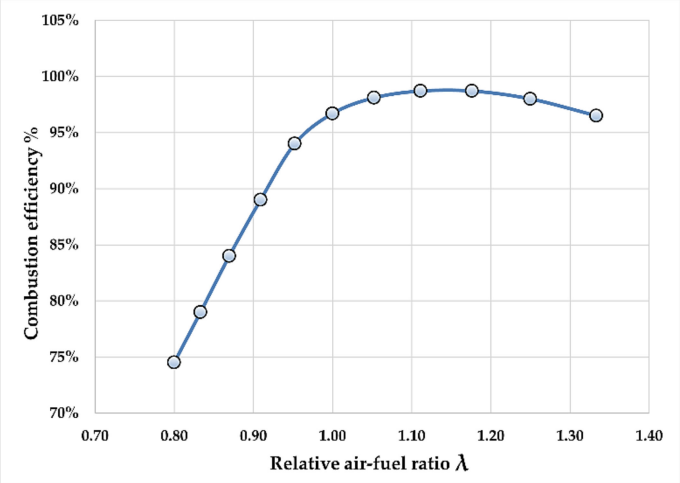

Figure 7. Spark ignition engines combustion efficiency as function of the relative air-fuel ratio λ.

For the determination of the chemical-physical properties of the natural gas, the authors employed the data provided by a local natural gas supplier (see Table 2). The data shown in Table 2 allow us to calculate the *CNG* relative fuel density (δ' = 0.64), and hence the gross indicated mean effective pressure of the *CNG*-fueled engine, for each operating condition.

Table 2. Composition and properties of the natural gas considered [26].

CNG Composition	**Percentage**
Methane—CH_4 [% mole of fuel]	86.49%
Ethane—C_2H_6 [% mole of fuel]	8.79%
Propane—C_3H_8 [% mole of fuel]	1.18%
Nitrogen—N_2 [% mole of fuel]	1.32%
Carbon dioxide—CO_2 [% mole of fuel]	1.89%
Other [% mole of fuel]	0.33%
CNG properties	**Value**
Specific gas constant—$R_{CNG}{}'$ [J·kg^{-1}·K^{-1}]	451.42
Lower Heating Value [MJ kg^{-1}]	46.93
Hydrogen/Carbon Ratio	3.78

The indicated mean effective pressure of the baseline *CNG* engine could then be evaluated through the *PMEP* of Equation (8):

$$IMEP_{CNG} = IMEP_{g,CNG} + (MAP - p_{S0}) \tag{15}$$

Since it is realistic to assume that the constants *A*, *B*, *C* and *D* of the *FMEP* model remain unchanged when changing the kind of fuel, the $FMEP_{CNG}$ was evaluated on the basis of the $IMEP_{CNG}$ through Equation (2). The $BMEP_{CNG}$ could be hence calculated as:

$$BMEP_{CNG} = IMEP_{CNG} - FMEP_{CNG} \tag{16}$$

and the resultant brake thermal efficiency, as well as brake specific fuel consumption, could be calculated as:

$$\eta_{b,CNG} = \frac{BMEP_{CNG} \cdot \left(\lambda \cdot \alpha_{st} + \frac{1}{\delta'}\right)}{\delta_A \cdot \lambda_V \cdot LHV_{CNG}} \tag{17}$$

$$BSFC_{CNG[\mathrm{g/kWh}]} = \frac{3600}{LHV_{CNG[\mathrm{MJ/kg}]} \cdot \eta_{b,CNG}} \quad (18)$$

With the aim being to pass from the normalized mean piston speed u to the effective mean piston speed u_m coherently with the technological level considered for the baseline naturally aspirated engine (European Type C–Medium vehicle), a maximum reference value of $u_{m(max)}$ = 17 m/s was assumed.

As a final result, Figure 8 shows the *BSFC* contour map obtained for the baseline *CNG* spark ignition engine as a function of the mean piston speed u_m and *BMEP*. The same figure also shows the full load *BMEP* of the *CNG*-fueled naturally aspirated engine. As already mentioned, each engine considered in this study was sized to provide the target maximum output power of 73.5 kW (100 HP); given the full load *BMEP* values of Figure 8, the necessary engine displacement *VA* of the *CNG*-fueled naturally aspirated engine was 1610 cc: Table 3 resumes the whole specifications of the baseline *CNG* spark ignition engine.

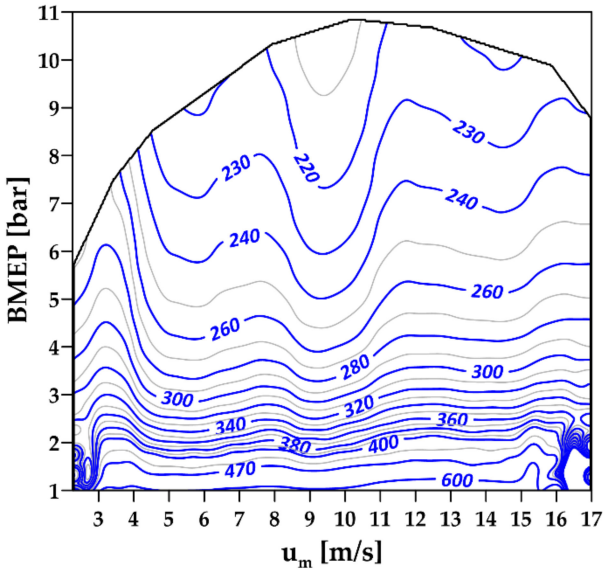

Figure 8. Brake specific fuel consumption map of the *CNG*-fueled naturally aspirated engine.

Table 3. Main characteristics of the baseline *CNG*-fueled S.I. naturally aspirated engine.

Engine	4-stroke, naturally aspirated, spark ignition
Displacement	1610 cc
Number of cylinders	4
Bore	77.28 mm
Stroke	85.78 mm
Max mean piston speed	17 m/s
Compression ratio	11
Injection system	CNG multi-point injection
Valvetrain	4 valves/cylinder, VVT
Max BMEP	10.85 bar at 3567 rpm
Max Power	73.5 kW at 5549 rpm
Min BSFC	206.8 g/kWh

3. Reference Turbocharged *CNG* Engine

As already mentioned, the advantages connected to the implementation of the separated electric compound SI *CNG* engine were compared with a reference traditional turbocharged *CNG* engine, whose performance is evaluated in this section. The scheme of the reference turbocharged *CNG* engine is represented in Figure 9: the turbocharger is composed of a turbine and a turbocompressor which are mechanically linked to each other, and both are fluid-dynamically connected to the engine. Figure 9 also shows the presence of a waste-gate valve for the turbine bypass, and an intercooler between the engine and the compressor for cooling down the air charge. Given the high knock resistance of natural gas [27,28] and the relatively low engine compression ratio adopted (i.e., 11), for the *CNG*-fueled turbocharged engine, a maximum boost pressure of 1.85 bar was assumed. Based on the specific parameters of the baseline *CNG* naturally aspirated engine, the performances of the turbocharged engine were then determined.

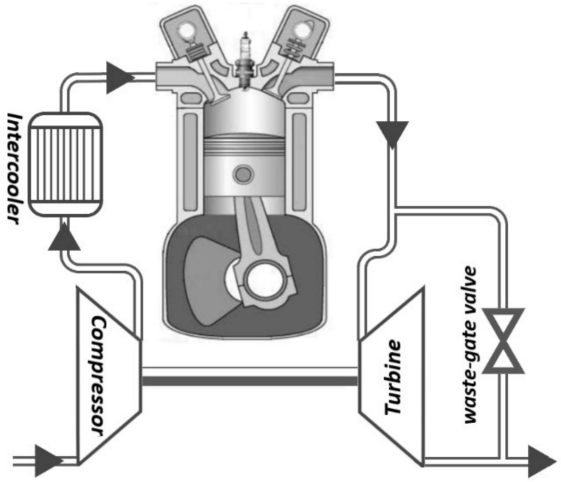

Figure 9. Scheme adopted for the reference turbocharged engine.

As a first step, the authors calculated the air mass flow to the engine, which, for each *MAP* and mean piston speed u_m, is:

$$G_T = \frac{V_T \cdot n}{60 \cdot \varepsilon} \cdot \delta_T \cdot \lambda_{V,T} \frac{\alpha}{\alpha + \frac{1}{\delta'}} \tag{19}$$

where V_T is the turbocharged engine displacement, n is the speed of rotation, $\lambda_{V,T}$ is the volumetric efficiency, and δ_T is the air density at the engine inlet, evaluated through the ideal gas law:

$$\delta_T = \frac{MAP}{R'_{air} \cdot T_T} \tag{20}$$

which in turns depends on the intercooler outlet temperature T_T and on the manifold absolute pressure *MAP*. The compressor outlet temperature was estimated as:

$$T_T{}' = T_0 \cdot \left(1 + \frac{\beta_C^{\frac{k_C - 1}{k_C}} - 1}{\eta_C} \right) \tag{21}$$

where η_C is the compressor adiabatic efficiency (whose evaluation is described further on), $\beta_C = p_C/p_0$ is the compression ratio, and k_C is the isentropic coefficient. Assuming a plausible intercooler efficiency value R_{INT} equal to 0.7, it was possible to determine the temperature of the air inlet to the engine:

$$T_T = T_T{}' - R_{INT}\left(T_T{}' - T_0\right) \tag{22}$$

The volumetric efficiency of the turbocharged *CNG* engine $\lambda_{V,T}$ was evaluated from the volumetric efficiency of the naturally aspirated *CNG* engine λ_{V0} for each mean piston speed u_m and corrected through two factors. The first correction considers the variation of the pressure difference between the engine inlet and exhaust, while the second is instead linked to the increased inlet temperature to the engine (which, as is known, increases the volumetric efficiency) due to the compression from the ambient to the turbocharging pressure. For the evaluation of the first correction factor, a simple approach usually adopted in academic courses was followed:

$$\frac{\lambda'_V(n)}{\lambda_V(n)} = 1 + \frac{MAP - p_S}{k \cdot MAP \cdot (\rho - 1)} \tag{23}$$

Obviously, this correction factor is unitary when no pressure difference exists between the inlet and the exhaust. Considering that the exhaust back pressure p_{S0} of the baseline naturally aspirated engine was assumed to be higher than the atmospheric pressure (p_{S0} = 1.1 p_0, as mentioned before), to take into account the variation of the difference between the inlet and exhaust pressure due to both *MAP* and p_S variation, the authors employed Equation (23) as follows:

$$\frac{\lambda_V(u_m)}{\lambda_{V0}(u_m)} = \frac{1 + \frac{MAP - p_S}{k \cdot MAP \cdot (\rho - 1)}}{1 + \frac{p_0 - p_{S0}}{k \cdot p_0 \cdot (\rho - 1)}} \tag{24}$$

where, as already mentioned, the volumetric efficiency λ_{V0} of the baseline naturally aspirated engine was considered at the exhaust pressure p_{S0} and at the manifold pressure p_0. As regards the second correction factor, which accounts for the increased inlet temperature due to compression, the authors adopted the classical relation:

$$\frac{\lambda_V(u_m)}{\lambda_{V0}(u_m)} = \sqrt{\frac{T_T}{T_0}} \tag{25}$$

Therefore, combining Equations (24) and (25), the volumetric efficiency $\lambda_{V,T}$ of the turbocharged engine was evaluated:

$$\lambda_{V,T}(u_m) = \lambda_{V,0}(u_m) \cdot \sqrt{\frac{T_T}{T_0}} \cdot \left[\frac{1 + \frac{MAP - p_S}{k \cdot MAP \cdot (\rho' - 1)}}{1 + \frac{p_0 - p_{S0}}{k \cdot p_0 \cdot (\rho - 1)}} \right] \tag{26}$$

In a turbocharged engine, as shown in Figure 9, the power required by the compressor P_{comp} to compress the air mass flow G_T is supplied by the turbine, whose power output is P_{turb}. The power balance is hence:

$$P_{comp} = P_{turb} \tag{27}$$

The power required by the turbocompressor is:

$$P_{comp} = G_T \cdot cp_C \cdot \frac{T_0}{\eta_C} \cdot \left(\beta_C^{\frac{k_C - 1}{k_C}} - 1 \right) \tag{28}$$

Additionally, the turbine output-power is:

$$P_{turb} = G_S \cdot cp_S \cdot \eta_S \cdot T_S \cdot \left(1 - \beta_S^{\frac{1 - k_S}{k_S}} \right) \tag{29}$$

where T_0 and T_S are the gas temperature at compressor and turbine inlet, respectively, cp_C and cp_S are the specific heat at a constant pressure of fresh air and exhaust gas, respectively,

η_S is the efficiency of the turbine (whose calculation procedure is described below), G_S is the turbine mass flow and β_S is the turbine pressure ratio. It is worth pointing out that the turbine pressure ratio β_S is defined as:

$$\beta_S = \frac{p_S - \Delta p_1}{p_0 + \Delta p_2} \tag{30}$$

where p_S is the in-cylinder gas pressure during exhaust stroke, Δp_1 is the pressure drop in the turbine inlet, and Δp_2 is the pressure drop between the turbine outlet and ambient pressure p_0; hence, the overall exhaust pressure drop from the cylinder to the ambient pressure is:

$$\Delta p_{TOT} = p_S - p_0 \tag{31}$$

In this paper, for simplicity purposes, the overall exhaust pressure drop was considered unchanged with respect to the baseline engine, and was composed of two equal parts, thus obtaining:

$$\Delta p_1 = \Delta p_2 = 0.5 \cdot \Delta p_{TOT} = 0.5 \cdot (p_{S0} - p_0) \tag{32}$$

Focusing on the turbocharger, the turbine mass flow G_S and the compressor mass flow G_T are connected through the relationship:

$$G_S = \Omega \cdot G_T \frac{\alpha + 1}{\alpha} \tag{33}$$

where the term $\left(\frac{\alpha+1}{\alpha}\right)$ is the fuel mass flow (which is added to the air mass flow downstream the compressor), while Ω represents the portion of exhaust mass flow that is not bypassed by the waste-gate valve (common values of Ω lie between 1 and 0.4). According to the power balance of Equation (27), the turbocharging compression ratio can be expressed as:

$$\beta_C = \left[1 + \Omega \cdot \frac{\alpha + 1}{\alpha} \cdot \frac{cp_S}{cp_C} \cdot \frac{T_S}{T_0} \cdot \eta_S \cdot \eta_C \cdot \left(1 - \frac{1}{\beta_S^{\frac{k_S - 1}{k_S}}} \right) \right]^{\frac{k_C}{k_C - 1}} \tag{34}$$

In the calculations performed, the parameter Ω related to the waste-gate opening was adaptively reduced to prohibit exceeding the maximum allowed value of compression ratio β_C (i.e., 1.85). For the evaluation of the exhaust gas temperature at the pressure p_S, another simple equation usually adopted in academic courses was adopted:

$$T_S = T_1 \cdot \frac{p_S}{MAP} \cdot \frac{(k_S - 1)}{k_S} + \frac{T_4}{T_1} \cdot \frac{1}{k_S} \tag{35}$$

where T_1 represents the inlet temperature at intake valve closure (IVC) of the turbocharged engine, whose value is assumed as being equal to the gas temperature at the intercooler outlet T_T, while T_4 is the in-cylinder gas temperature at the exhaust valve opening (EVO) and k_S is the isentropic coefficient of the exhaust gas. The experimental data and scientific literature report, for a spark ignition engine, values of the ratio T_4/T_1 ranging from 3.5 to 4.5, depending on the particular engine and on the operating condition. In this work, the temperature ratio T_4/T_1 was assumed to remain constant, separate from engine load and speed. However, with the aim of investigating the effects of its variation on the performance of the whole system, three different values were selected, i.e., T_4/T_1 = 3.5, 4.0 and 4.5, and the entire calculation procedure was repeated for each of the three values.

The isentropic coefficient k_S was evaluated according to the perfect gas hypothesis:

$$k_S = \frac{c_{p,S}(T_S)}{c_{v,S}(T_S)} \tag{36}$$

$$c_{v,S}(T_S) = c_{p,S}(T_S) - R_S{}' \tag{37}$$

where $R_S{}'$ is the burned gas constant and $c_{v,S}$ is the constant volume specific heat (evaluated at the exhaust gas temperature T_S). Obviously, the thermochemical properties of the burned gas were calculated as weighted averages on the basis of the chemical composition, i.e.,

$$c_{p,S} = c_{p,CO_2}(T_S) \cdot x_{CO_2} + c_{p,H_2O}(T_S) \cdot x_{H_2O} + c_{p,N_2}(T_S) \cdot x_{N_2} \tag{38}$$

$$R'_S = R'_{CO_2} \cdot x_{CO_2} + R'_{H_2O} \cdot x_{H_2O} + R'_{N_2} \cdot x_{N_2} \tag{39}$$

where x is the mass fraction of each chemical species in the burned gas: for this purpose, the combustion of a hydrocarbon with H/C = 3.78 was considered for the calculation of each mass concentration (see Table 2). It is worth noting that in both Equations (38) and (39), no carbon monoxide is considered, due to the assumption that the *CNG*-powered engine was never fueled with rich air–fuel mixtures. The constant-pressure specific heat of each chemical species in the burned gas was evaluated as a function of the exhaust gas temperature T_S through the Shomate equations and the coefficients available on the NIST Chemistry WebBook [29].

The calculation of the power produced by the turbine requires the turbine characteristic curves correlating the pressure ratio to the gas mass flow for each speed of rotation. According to the simple approach followed in this model, a single fitting curve was adopted to describe the turbine mass flow parameter MFP as a function of the pressure ratio β_S, whose mathematical expression is:

$$MFP = \frac{a \cdot b + c \cdot \beta_S^d}{b + \beta_S^d} \tag{40}$$

The values of the function parameters a, b, c and d were obtained by means of a least square regression procedure performed on the performance data of a market available product (IHI RHF3). The turbine mass flow G_S could then be obtained from the *MFP*:

$$G_S = MFP \frac{p_S}{\sqrt{T_S}} \tag{41}$$

Since, in the calculations performed, the engine size was iteratively determined on the basis of the specific performance obtained, the *MFP* curve of Equation (40) was amplified or reduced in order to adapt the turbine size and swallowing capacity to the displacement and performance of the engine under analysis: as an example, Figure 10 shows the *MFP* curves related to three different turbine sizes. The data available on the mentioned commercial product also allowed us to express the turbine efficiency as a function of the pressure ratio β_S by means of the polynomial function:

$$\eta_S = -\frac{292.1}{10^4}\beta_S^5 + \frac{3933}{10^4}\beta_S^4 - 2.049\beta_S^3 + 5.113\beta_S^2 - 6.072\beta_S + 3.321 \tag{42}$$

The resulting efficiency curve η_S is also reported in Figure 10.

The performance map of the IHI RHF3 series turbocharger was also used for the evaluation of the compressor efficiency η_C. As performed for the turbine, an iterative resizing procedure was also carried out to best adapt the compressor size to the engine. For this aim, the turbocharger map was recursively adapted by modifying the minimum and maximum values on both axes (β_C, G_T), thus maintaining the compressor operating points within the scaled map, as shown in Figure 11. The calculation of the operating parameters of the turbocharger thus requires, for each mean piston speed u_m (from 2.3 to 17.0 m/s) and *MAP* (from 0.78 bar up to 1.85 bar), the recursive solution of Equations (23)–(42). Once the system of equations is solved, the conditions of the gas at the engine inlet and outlet are known, and then the performance of the turbocharged engine may be evaluated. The

described iterative adaptation of the turbocharger size represents the procedure usually employed when selecting and matching a turbocharger to a specific engine.

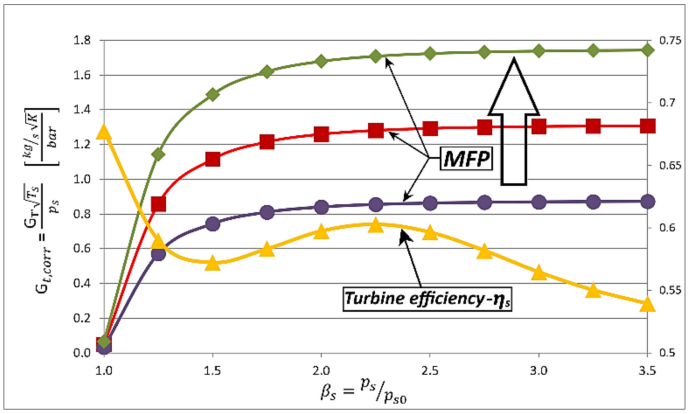

Figure 10. Performance of the exhaust gas turbine (mass flow parameter and efficiency as a function of pressure ratio).

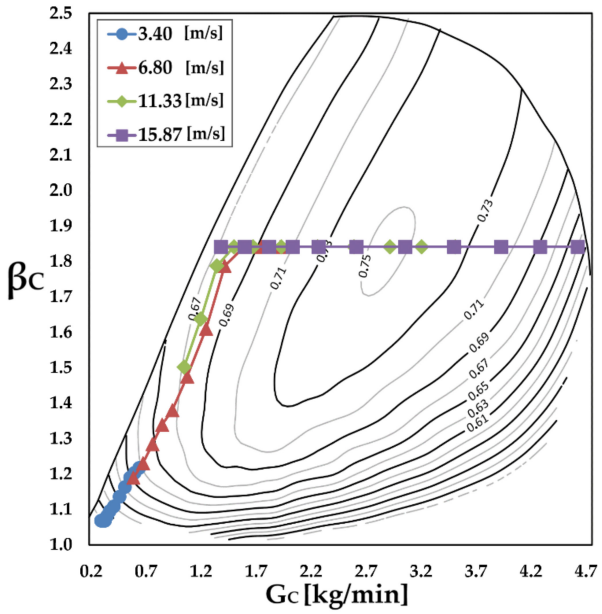

Figure 11. Turbocharger performance map reporting the operating points obtained for every engine load and four mean piston speeds.

As a starting hypothesis for the mathematical modeling of the turbocharged engine, the authors assumed that the same gross indicated efficiency is obtained at the same normalized *MAP* and mean piston speed, even with different absolute manifold pressures. This is obviously a simplified assumption which underestimates the efficiency of the turbocharged engine, which should instead be slightly higher with respect to the naturally aspirated version.

Defining the normalized *MAP* as:

$$\phi = \frac{MAP}{MAP_{\max}} \tag{43}$$

according to the hypothesis made, the gross indicated efficiency of the turbocharged engine $\eta_{ig,T}$ was determined starting from the gross indicated efficiency of the naturally aspirated engine $\eta_{ig,CNG}$:

$$\eta_{ig,T}(\phi, u_m) = \eta_{ig,CNG}(\phi, u_m) \tag{44}$$

Once we established the gross indicated efficiency for each operating point, it was possible to obtain the gross indicated mean effective pressure $IMEP_{g,T}$ of the turbocharged engine as:

$$IMEP_{g,T} = \frac{\delta_T \cdot \lambda_{V,T} \cdot LHV}{\alpha + \frac{1}{\delta'}} \cdot \eta_{ig,T} \quad (45)$$

In turn, the net indicated mean effective pressure $IMEP_T$ was calculated as:

$$IMEP_T = IMEP_{g,T} + PMEP_T \quad (46)$$

while the pumping mean effective pressure $PMEP_T$ was simply calculated as:

$$PMEP_T = MAP - p_S \quad (47)$$

With the friction mean effective pressure still being represented by Equation (2) adopted for the naturally aspirated engine, the authors determined the brake mean effective pressure $BMEP_T$ of the turbocharged engine:

$$BMEP_T = IMEP_T + FMEP_T \quad (48)$$

and the corresponding brake specific fuel consumption $BSFC_T$:

$$BSFC_T = \frac{\delta_T \cdot \lambda_{V,T}}{BMEP_T \cdot \left(\alpha + \frac{1}{\delta'}\right)} \quad (49)$$

As performed in the case of the naturally aspirated engine, the full load $BMEP_T$ values were used to size the displacement V_T of the turbocharged engine necessary to develop the maximum target output power of 73.5 kW. As already pointed out, the entire calculation procedure described in this paragraph was repeated for each assumed value of the temperature ratio T_4/T_1 (i.e., 3.5, 4.0 and 4.5). Table 4 reports the main characteristics and performances determined for the turbocharged *CNG*-fueled engine according to the three temperature ratios T_4/T_1. A contour map of the brake specific fuel consumption obtained for the intermediate case of T_4/T_1 = 4 is reported in Figure 12.

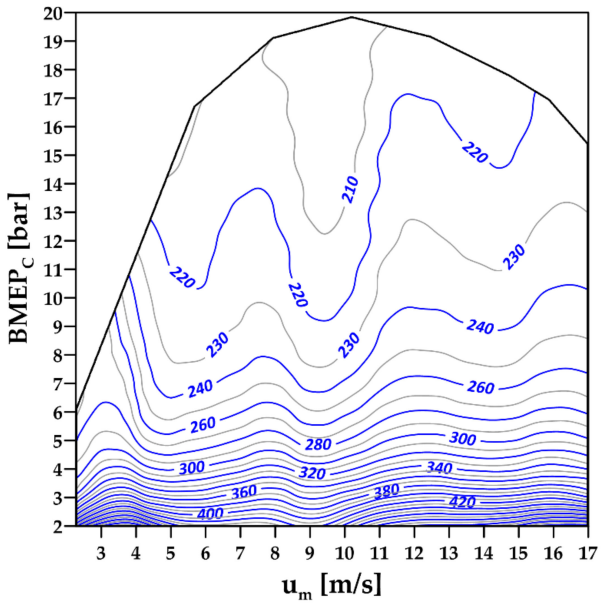

Figure 12. Brake specific fuel consumption map of the reference turbocharged engine with T_4/T_1 = 4.

Table 4. Main characteristics of the reference turbocharged engine evaluated for each of the three temperature ratios T_4/T_1.

Engine	4-stroke, spark ignition		
Injection system	CNG- multi-point injection		
Compression ratio	11		
Valvetrain	4 valves/cylinder, VVT		
Max mean piston speed	17 m/s		
T_4/T_1	3.5	4.0	4.5
Number of cylinders	3	3	3
Displacement [cc]	890 cc	826 cc	781 cc
Bore	69.8 mm	68.1 mm	66.8 mm
Stroke	77.5 mm	75.6 mm	74.2 mm
Max BMEP	19.5 bar at 3950 rpm	19.9 bar at 4050 rpm	20.1 bar at 4120 rpm
Max Power	73.5 kW at 6140 rpm	73.5 kW at 6300 rpm	73.5 kW at 6420 rpm
Min BSFC	201.2 g/kWh	199.3 g/kWh	197.9 g/kWh

4. Separated Electric Compound Spark Ignition Engine

This section describes the calculation algorithm developed to evaluate the performance of the proposed compound engine, which will finally be compared with the reference turbocharged engine developed in the previous section. Figure 2c shows the schematic representation of the compound system proposed in this work, composed of a spark ignition engine supercharged by an electrically powered turbocompressor, and endowed with a turbine generator group dedicated to recovering the unexpanded gas energy of the exhaust gas; Figure 3, meanwhile, reports a possible hybrid architecture endowed with the compound engine: as already clarified, in the system conceived in this paper, the energy recovered by the turbine generator is stored in the energy storage system of the vehicle and used for vehicle propulsion. As can also be noted in Figure 2c, a bypass valve between the compressor inlet and outlet allows us to power off the compressor in the part load operation, when an *MAP* lower than 1 bar is required, thus reducing the power absorption of the supercharging system. As already pointed out, the turbine generator group is instead considered to operate permanently, in order to recover as much energy as possible from the exhaust gas. As regards the sizing of the turbocompressor, the authors followed the same procedure and calculation algorithm already described in the previous section for the reference turbocharged engine. It is worth noting that the authors hypothesized the use of a turbocompressor, it being the most commonly used tool of its kind in the automotive field; however, nothing prevents the adoption of a different machine, such as a Roots type or a screw compressor. It must be also pointed out that the turbine considered for this application substantially differs from the turbines commonly employed for turbocharging purposes, which only provide the power necessary to drive the compressor and are designed to comply with wide variations of speed and mass flow, thus not being optimized for steady state operation. For this reason, the turbines developed for turbocharging application are low-inertia single-radial stage machines, with conversion efficiencies far below the values reached by turbines used in stationary systems. As will be shown later on, the turbine considered in this work will have to deliver powers up to 23 kW, which is why it should be composed of more than a single stage (two or more), in order to recover the exhaust energy content with higher efficiency than common turbocharging turbines. Moreover, as already mentioned, the exhaust gas turbine employed in a hybrid propulsion system should work under almost steady state conditions, which is why a torque/current control on the generator would allow the machine to operate at its best efficiency speed ratio, regardless of the power produced. The only turbine generator

products present on the market or studied until now are composed of a radial turbine for turbocharging applications connected to an electric generator [30–32], and are designed exclusively to supply the vehicle's electric accessories, thus producing a very limited power output (i.e., 6 kW). Due to the lack of adequate products both in the literature and on the market, and according to the previous considerations, the authors assumed that in the compound engine, the turbine works with an almost constant speed ratio, regardless of the power produced, and hence with an almost constant efficiency η_T. Given the lack of previous studies, it was not possible to exactly predict the effective efficiency of the exhaust gas turbine: on account of this, the authors decided to consider two different efficiency levels, thus assessing the effect of this parameter on the overall energetic performance of the entire compound system. In detail, the two levels of efficiency considered for the compound engine turbine are $\eta_T = 0.70$ and $\eta_T = 0.75$. As already mentioned, the two efficiency values of the exhaust gas turbine are substantially higher than a common turbocharging turbine, due to the dedicated and optimized design for steady state power production.

As already conducted in the case of the reference turbocharged engine, the performances of the compound engine were evaluated for each *MAP* (from 0.78 bar to the maximum allowed 1.85 bar) and mean piston speed u_m (from 2.3 to 17.0 m/s). The gross indicated mean effective pressure of the compound engine was evaluated as:

$$IMEP_{g,COMP} = \frac{\delta_{COMP} \cdot \lambda_{V,COMP} \cdot LHV}{\alpha + \frac{1}{\delta^l}} \cdot \eta_{ig,COMP} \quad (50)$$

where the inlet air density δ_{COMP} of the compound engine was evaluated by means of Equations (20)–(22). For the evaluation of both the indicated gross efficiency $\eta_{ig,COMP}$ and the volumetric efficiency $\lambda_{V,COMP}$, some observations are necessary, considering that the exhaust gas turbine will produce an increase in the exhaust gas back pressure p_S. Differing from a traditional turbocharged engine, the effect of the increased exhaust back pressure will certainly be stronger in the compound engine for two main reasons: firstly, because unlike the traditional system, in the proposed compound system, the exhaust gas turbine works with the whole exhaust mass flow with a relatively high pressure ratio $\beta_S = p_S/p_{S0}$ (as will be shown later). Secondly, the expander-generator unit is considered to remain permanently active, i.e., also for the partial load operation, when the engine *MAP* is lower than 1 bar. As is widely known, an increase in the engine exhaust back pressure affects both the indicated gross efficiency and the volumetric efficiency. As concerns the volumetric efficiency, a higher exhaust back pressure causes a higher residual gas mass inside the cylinder, thus limiting the amount of fresh mass that can be introduced during the intake phase. This phenomenon was taken into consideration by means of Equation (26), which correlates the volumetric efficiency to the pressure difference between intake and exhaust. Alternatively, as regards the indicated engine efficiency, it is known that a higher in-cylinder residual gas fraction (*RGF*) will certainly slow down the flame propagation speed and worsen the combustion efficiency; however, no useful mathematical expressions were found in the scientific literature to represent the indicated efficiency deterioration as a function of the exhaust back pressure: on account of this lack of mathematical expressions, the authors performed a dedicated series of experimental tests on a bench test (whose detailed description may be found in [33,34]) equipped with a 1.242 L port injected spark ignition engine fueled with *CNG* and connected to a Schenck W130 eddy current dynamometer; a throttle valve installed in the exhaust pipe was used to modulate the exhaust back pressure, and an AVL GU13X piezoelectric pressure sensor flush mounted in the engine combustion chamber was employed for the in-cylinder pressure measurement, performed with a sample resolution of 1 CAD through the use of a 360 ppr optical encoder connected to the engine crankshaft. The exhaust pressure was evaluated as the average in-cylinder pressure during the exhaust stroke, excluding the blowdown period. The air mass flow was measured by means of an FCI ST75 mass flow meter, while natural gas mass flow measurement was performed using an Endress + Hauser Coriolis effect PROMASS 80A; an ECM AFRecorder 2400 module was employed to measure both the manifold absolute

pressure and engine speed. Table 5 resumes the operating condition of the test: as is shown, for each engine speed, the exhaust pressure was increased with steps of 0.1 bar until the occurrence of heavy combustion instability (identified by misfires occurrence), and without exceeding the maximum level of 2 bar. Table 6 instead reports the measurement accuracy of the instrumentation employed in the experimental test.

Table 5. Operating conditions of the experimental test.

Engine speed (rpm)	1500–2500–3500
MAP (bar)	1
Exhaust pressure p_S (bar)	1.0 to 2.0 in steps of 0.1
Fuel	CNG
Spark advance	Optimal (LPP = 15° ATDC)
Air–fuel ratio	Stoichiometric

Table 6. Measurement accuracy of the instrumentation employed in the test.

Sensor	**Accuracy**
MAP	±1% FSO (2.38 bar)
Engine speed	±10 rpm
NG mass flow	±1% of reading
Air mass flow	±2% reading, ±0.5% full scale
Engine torque	±2% of reading
In-cylinder pressure	linearity error < ±0.3% FSO
In-cylinder pressure	thermal sensitivity shift ≤ ±0.5% at temperature between 200 and 300 °C

The experimental measurements showed that there is a correlation between the increase in the residual gas fraction (defined as the ratio between the residual gas mass and the total in-cylinder mass of gas) and the decrease in the gross indicated efficiency, whose best fit was obtained by the equation:

$$\frac{\eta_{i,g}}{\eta_{i,g,0}} = \frac{1}{1 + b \cdot x^{\gamma}} \tag{51}$$

where $\left(\frac{\eta_{i,g}}{\eta_{i,g,0}}\right)$ is the ratio between the indicated gross efficiencies measured with and without exhaust throttling, while $x = RGF/RGF_0$ is the ratio between the residual gas fractions detected with and without exhaust throttling; the parameters b and γ are correlated with the mean piston speed, which, as shown in Figure 13, has a strong influence on the efficiency variation.

$$b = 0.1384 \cdot {u_m}^{-2.635} \tag{52}$$

$$\gamma = -0.2556 \cdot u_m + 6.0391 \tag{53}$$

Each residual gas fraction RGF was estimated through the procedure described in Appendix A.

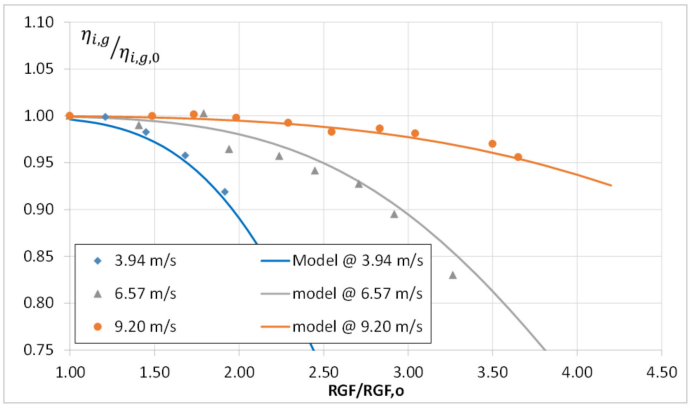

Figure 13. Variation of the engine gross indicated efficiency as a function of the RGF ratio.

With the same approach followed for the reference turbocharged engine, it was assumed that the gross indicated efficiency is the same for the same engine and the same conditions of normalized *MAP* ϕ and mean piston speed u_m. According to this assumption, the reference gross indicated efficiency of the compound engine $\eta_{i,g,COMP,0}$ (i.e., without exhaust throttling) was evaluated as:

$$\eta_{ig,COMP,0}(\phi, u_m) = \eta_{ig,CNG}(\phi, u_m) \tag{54}$$

The residual gas fraction *RGF* and the resulting gross indicated efficiency $\eta_{i,g,COMP}$ of the supercharged compound engine could hence be determined for each *MAP* and mean piston speed on the basis of the exhaust gas back pressure p_S through Equations (51)–(53). The gross indicated mean effective pressure could be then calculated using Equation (50), which, in turn, allowed us to evaluate the compound engine net indicated mean effective pressure $IMEP_{COMP}$:

$$IMEP_{COMP} = IMEP_{g,COMP} + PMEP_{COMP} \tag{55}$$

with the pumping mean effective pressure $PMEP_{COMP}$ being estimated through Equation (47), as in the case of the reference turbocharged engine. Equation (2) was then employed to evaluate the $FMEP_{COMP}$, and hence the engine $BMEP_{COMP}$ was obtained from Equation (48).

Unlike the previous cases, however, in the compound system, the exhaust gas turbine actively contributes to the energy production, and so the total output power results from the sum of the engine and the turbine contributions. The overall brake mean effective pressure of the whole compound system $BMEP_{TOT}$ can hence be obtained as:

$$BMEP_{TOT} = BMEP_{COMP} + RMEP - CMEP \tag{56}$$

where *RMEP* is the recovery mean effective pressure of the exhaust gas turbine and *CMEP* is the compression mean effective pressure, derived from the power required by the motor-compressor. The recovery mean effective pressure *RMEP* was estimated as:

$$RMEP = \frac{60 \cdot \varepsilon \cdot P_{tur}}{V_{COMP} \cdot n} \tag{57}$$

where P_{tur} is the power produced by the exhaust gas turbine, V_{COMP} is the displacement of the compound engine and ε is the number of engine revolutions per cycle (two in a four-stroke engine). Analogously, the compression mean effective pressure was calculated as:

$$CMEP = \frac{60 \cdot \varepsilon \cdot P_{comp}}{V_{COMP} \cdot n \cdot \eta_{EM}} \tag{58}$$

where P_{comp} is the power required by the compressor and η_{EM} is the electric motor efficiency. As can be noted, the efficiency of the electric motor driving the compressor was considered, the motor-compressor group being an auxiliary device which affects the system energy balance; the efficiency of the turbine electric generator was not considered in the *RMEP* (Equation (57)) with the calculation performed for the output power from the internal combustion engine, which was not reduced by the efficiency of the connected electric generator (MG1 in Figure 3).

The power required by the compressor and the power produced by the turbine were evaluated as in the previous paragraph:

$$P_{comp} = G_{COMP} \cdot cp_C \cdot \frac{T_0}{\eta_C} \cdot \left(\beta_C^{\frac{k_C - 1}{k_C}} - 1 \right) \tag{59}$$

$$P_{tur} = G_{COMP} \cdot \frac{\alpha + 1}{\alpha} \cdot cp_S \cdot \eta_T \cdot T_S \cdot \left(1 - \beta_S^{\frac{1 - k_S}{k_S}} \right) \tag{60}$$

With the exception being that the intake air mass flow of the compound engine is now G_{COMP}, while the exhaust gas turbine efficiency is indicated with η_T, all the other parameters (e.g., T_S, α, β_S, β_C, k_S, k_C, cp_C, $cp_{S,}$ etc.) have the same meaning as in the previous paragraph (Equations (28) and (29)). It is worth noting that, as in this case the expander is supposed to permanently work with the entire exhaust gas mass flow, no bypass exists, and hence the term Ω is considered to equal 1.

The engine intake air mass flow is:

$$G_{COMP} = \frac{V_{COMP} \cdot n}{60 \cdot \varepsilon} \cdot \delta_{COMP} \cdot \lambda_{V,COMP} \frac{\alpha}{\alpha + \frac{1}{\delta'}} \tag{61}$$

The specific performance parameters *RMEP* and *CMEP* hence become:

$$RMEP = \frac{60 \cdot \varepsilon}{V_{COMP} \cdot n} \cdot G_{COMP} \cdot \frac{\alpha + 1}{\alpha} \cdot c_{p,S} \cdot T_S \cdot \eta_T \cdot \left(1 - \beta_S^{\frac{1 - k_S}{k_S}} \right) \tag{62}$$

$$CMEP = \frac{60 \cdot \varepsilon}{V_{COMP} \cdot n \cdot \eta_{EM}} \cdot G_{COMP} \cdot cp_C \cdot \frac{T_0}{\eta_C} \cdot \left(\beta_C^{\frac{k_C - 1}{k_C}} - 1 \right) \tag{63}$$

After determining the overall brake specific performance $BMEP_{TOT}$ for each operating condition of *MAP* and mean piston speed u_m, the overall brake thermal efficiency η_{bTOT} of the compound system can be calculated as:

$$\eta_{bTOT} = \frac{BMEP_{TOT} \cdot \left(\alpha + \frac{1}{\delta'} \right)}{\delta_{COMP} \cdot \lambda_{V,COMP} \cdot LHV} = \frac{(BMEP_{COMP} + RMEP - CMEP) \cdot \left(\alpha + \frac{1}{\delta'} \right)}{\delta_{COMP} \cdot \lambda_{V,COMP} \cdot LHV} \tag{64}$$

Hence, the related overall brake specific fuel consumption $BSFC_{TOT}$ is:

$$BSFC_{TOT} = \frac{\delta_{COMP} \cdot \lambda_{V,COMP}}{BMEP_{TOT} \cdot \left(\alpha + \frac{1}{\delta'} \right)} \tag{65}$$

It must be pointed out that if, on the one hand, a higher discharge pressure increases the recovery mean effective pressure *RMEP*, on the other hand, it also increases the pumping mean effective pressure $PMEP_C$ (Equation (47)) and worsens the gross indicated thermal efficiency, due to the increased amount of residual gas (Equation (51)); it is therefore evident that, for each engine load (*MAP*) and mean piston speed (u_m), there will be a compromise solution between the advantages and disadvantages resulting from increasing the exhaust back pressure p_S: in other words, for each operating point of the engine, an optimum

exhaust pressure exists which maximizes the overall brake thermal efficiency η_{bTOT} of the compound system.

In their calculations, the authors thus carried out an optimization process, searching, for each operating point of the engine, for the best exhaust back pressure p_S by maximizing the overall brake thermal efficiency η_{bTOT}; since the latter is not a linear or polynomial function of the exhaust pressure, a genetic algorithm was employed for system efficiency optimization. As already done in the case of the turbocharged engine, the entire calculation procedure was repeated for each value of the temperature ratio T_4/T_1 (namely 3.5, 4.0 and 4.5) and, in addition, for each value of the exhaust gas turbine efficiency η_T considered (i.e., 0.70 and 0.75). It is worth highlighting that, differing from the present paper, in the preliminary work [22], the authors limited their investigation to a single T_4/T_1 ratio and a single turbine efficiency value.

Figure 14 reports the contour maps of the optimal exhaust pressure levels determined for each overall load $BMEP_{TOT}$ and mean piston speed u_m, considering the case of $T_4/T_1 = 4.5$, $\eta_T = 0.75$.

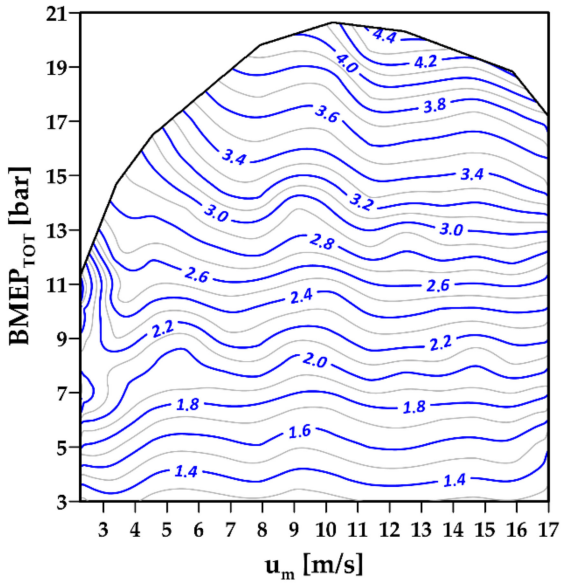

Figure 14. Optimal exhaust pressure levels as function of load and speed ($T_4/T_1 = 4.5$, $\eta_T = 0.75$).

As is shown, higher exhaust back pressures were obtained for the medium to higher loads, where the higher in-cylinder pressures make the recovery of the unexpanded gas energy easier. As can also be observed, optimal exhaust pressures up to 4.4 bar were determined for the extreme case of $T_4/T_1 = 4.5$ and $\eta_T = 0.75$, while in the extreme opposite case ($T_4/T_1 = 3.5$, $\eta_T = 0.70$), optimal exhaust pressures up to 3.4 bar were reached; both scenarios, however, revealed exhaust pressure values significantly higher than in a traditional turbocharged engine: these conditions must be adequately considered for the future optimal design of the exhaust gas turbine dedicated to the unexpanded gas energy recovery. The optimization process led to the determination of the maximum $BMEP_{TOT}$ levels for each design case, and, as a consequence, of the compound engine displacement V_{COMP} necessary to develop the maximum target power of 73.5 kW. The resulting main characteristics of the compound engine for each of the three temperature ratios T_4/T_1 considered are summarized in Table 7 for case study $\eta_T = 0.7$, and in Table 8 for the case study $\eta_T = 0.75$. The comparison of these results with the performance obtained by the traditional turbocharged engine (see Table 4) allows us to observe that the minimum fuel consumption is always lower in the electric compound engine.

Table 7. Main characteristic of the compound engine obtained with $\eta_T = 0.7$.

Engine	4-stroke, spark ignition		
Injection system	CNG multi-point injection		
Valvetrain	4 valves/cylinder, VVT		
Compression ratio	11		
Max boost pressure	1.85 bar		
Turbine efficiency	0.7		
Number of cylinders	3		
Stroke/bore ratio	1.11		
Displacement [cc]	731.1	708.9	695.6
T_4/T_1	3.5	4	4.5
Max $BMEP_{TOT}$	20.11 bar at 4220 rpm	20.34 bar at 4260 rpm	20.51 bar at 4290 rpm
Max output power	73.5 kW at 6560 rpm	73.5 kW at 6630 rpm	73.5 kW at 6670 rpm
Min $BSFC_{TOT}$	189.2 g/kWh	184.4 g/kWh	179.5 g/kWh
Variation of min BSFC	−6.33%	−8.09%	−10.25%
Max RMEP	4.18 bar at 5150 rpm	4.98 bar at 5210 rpm	5.86 bar at 5240 rpm
Max $RMEP/BMEP_{TOT}$	24.20%	29.70%	36.40%
Max expander power	15.16 kW at 6560 rpm	17.82 kW at 6630 rpm	21.00 kW at 6670 rpm

Table 8. Main characteristic of the compound engine obtained with $\eta_T = 0.75$.

Engine	4-stroke, spark ignition		
Injection system	CNG multi-point injection		
Valvetrain	4 valves/cylinder, VVT		
Compression ratio	11		
Max boost pressure	1.85 bar		
Turbine efficiency	0.75		
Number of cylinders	3		
Stroke/bore ratio	1.11		
Displacement [cc]	728.3	697.9	689.3
T_4/T_1	3.5	4	4.5
Max $BMEP_{TOT}$	20.09 bar at 4220 rpm	20.47 bar at 4280 rpm	20.66 bar at 4300 rpm
Max output power	73.5 kW at 6570 rpm	73.5 kW at 6660 rpm	73.5 kW at 6690 rpm
Min $BSFC_{TOT}$	186.7 g/kWh	181.5 g/kWh	176.2 g/kWh
Variation of min BSFC	−7.76%	−9.85%	−12.32%
Max RMEP	4.74 bar at 5160 rpm	5.53 bar at 5230 rpm	6.59 bar at 5250 rpm
Max $RMEP/BMEP_{TOT}$	28.40%	33.90%	42.90%
Max expander power	17.44 kW at 6570 rpm	19.64 kW at 6660 rpm	23.30 kW at 6690 rpm

In greater detail, a reduction in the minimum brake specific fuel consumption of between 6.33% (in the worst case $T_4/T_1 = 3.5$ and $\eta_T = 0.7$) and 12.32% (in the best solution case $T_4/T_1 = 4.5$ and $\eta_T = 0.75$) can be noted. The contour maps of the overall specific fuel con-

sumption $BSFC_{TOT}$ obtained for the two intermediate cases with $T_4/T_1 = 4.0$, $\eta_T = 0.7$ and $T_4/T_1 = 4.0$, $\eta_T = 0.75$ are shown in Figures 15 and 16, respectively. As obviously expected, the two diagrams confirm that the overall fuel consumption of the compound system benefits from a higher turbine efficiency. Comparison between the maps in Figures 15 and 16 with the fuel consumption map of the reference turbocharged engine (Figure 12) also allows us to observe that both propulsion solutions show similar *BMEP* values, but the compound system always exhibits a better fuel economy compared to the reference traditional turbocharged system.

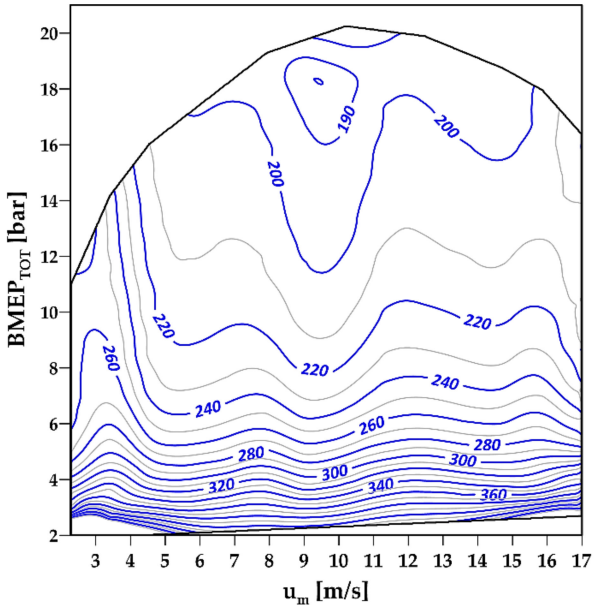

Figure 15. Brake specific fuel consumption (g/kWh) of the compound engine, as a function of the overall load and mean piston speed ($T_4/T_1 = 4.0$, $\eta_T = 0.70$).

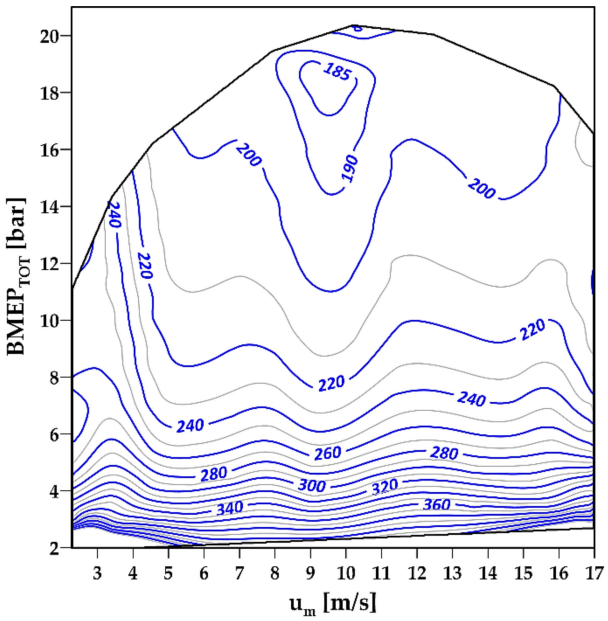

Figure 16. Brake specific fuel consumption (g/kWh) of the compound engine, as a function of the overall load and mean piston speed ($T_4/T_1 = 4.0$, $\eta_T = 0.75$).

Tables 7 and 8 also show the percentage contribution of the exhaust gas turbine to the overall output power of the compound system, revealing a maximum power share from

24.2% to 42.9%, with the higher results being obtained with the better efficiency turbine (η_T = 0.75): according to the modelling approach followed, the power contribution of the exhaust gas turbine to the vehicle propulsion would hence be relevant; as can also be observed in Tables 7 and 8, in the optimized system, maximum recovery mean effective pressures between 4.18 and 6.59 bar were determined, and the maximum power delivered by the exhaust gas turbine was calculated as being between 15.16 and 23.30 kW: once again, the higher values were obtained when the best-efficiency turbine (η_T = 0.75) was considered. All these results confirm that, if adequately recovered, the unexpanded exhaust gas energy may constitute a relevant part of the whole propulsion energy, thus helping to reduce both vehicle fuel consumption and related emissions.

The comparison based only on the minimum specific fuel consumption of the system is not exhaustive and provides a limited representation of the real beneficial effects of the separated electric compound propulsion system. Considering that in a hybrid propulsion system, the thermal unit is dedicated to producing the power required for both the vehicle traction and battery charging, the two propulsive solutions should be compared on an equal output power basis. For this purpose, the authors evaluated the overall efficiency improvement of the compound system with respect to the reference turbocharged engine for the same power output and the same mean piston speed; Figures 17 and 18 show the results obtained for the two extreme cases (T_4/T_1 = 3.5, η_T = 0.70 and T_4/T_1 = 4.5, η_T = 0.75). As can be seen, the major energetic benefits of the electric compound system are obtained in the high-load/speed regions; this can be easily explained considering that higher engine power implies higher in-cylinder pressures and exhaust mass flows: in these conditions, the turbine can provide a greater contribution to the overall output power of the system without compromising the engine's indicated efficiency, leading to greater exhaust gas energy recovery.

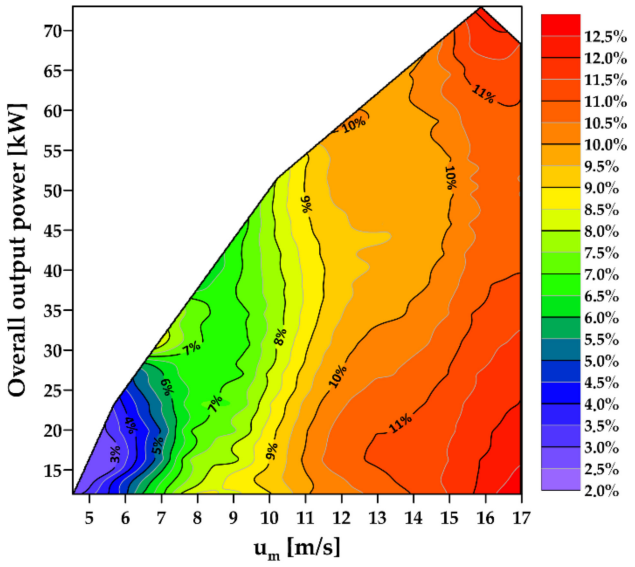

Figure 17. Efficiency improvement of the compound engine with respect to the reference turbocharged engine as a function of power output and mean piston speed for T_4/T_1 = 3.5 and η_T = 0.70.

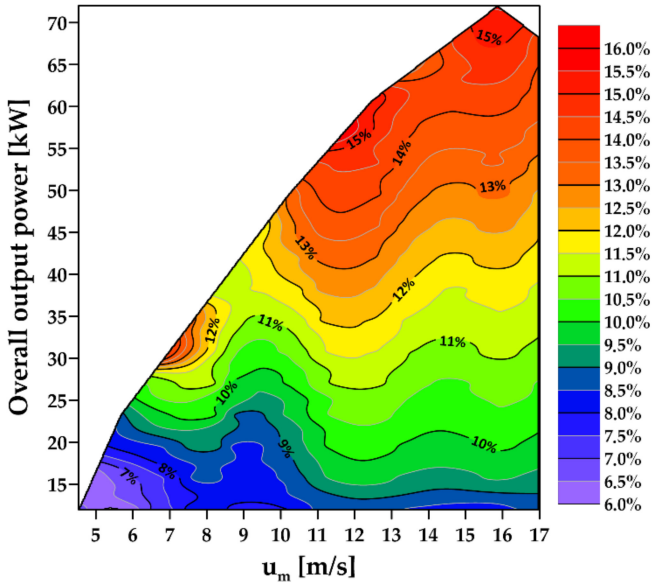

Figure 18. Efficiency improvement of the compound engine with respect to reference turbocharged engine as function of power output and mean piston speed for $T_4/T_1 = 4.5$ and $\eta_T = 0.75$.

At partial load, meanwhile, the recovery of the exhaust gas energy may not be energetically convenient; in these conditions, differing from a traditional turbocharged engine endowed with a waste-gate valve, the compound system can theoretically decrease the exhaust pressure down to the ambient pressure through an appropriate control in the turbine generator system. In greater detail, the efficiency improved by between 3% and 7% for the minimum power levels, reaching a maximum of about 12.5% in the case of Figure 17 ($T_4/T_1 = 3.5$, $\eta_T = 0.70$) and 15.5% in Figure 18 ($T_4/T_1 = 4.5$, $\eta_T = 0.75$) for the maximum power output levels. As can be expected, the best efficiency improvements were obtained with better turbine efficiency ($\eta_T = 0.75$) and a higher temperature ratio ($T_4/T_1 = 4.5$). For this reason, a correct study and optimization of the whole compound engine should be carried out with the aim to maximize the energetic advantages. The authors consider the results obtained to be very encouraging, especially if it is noted that the effect of the increased exhaust back pressure was not accounted for in the evaluation of the gross indicated efficiency of the reference turbocharged engine.

In a hybrid propulsion system, the operating point of the thermal unit is usually close to the best efficiency curve, i.e., the curve connecting the operating conditions which ensure, for each power request, the maximum efficiency; on account of this consideration, the authors carried out a further, and fairer, comparison, based on the best efficiency curves of both the compound engine and the reference turbocharged engine. For this purpose, for each power output, the authors evaluated the best operating conditions (i.e., with best efficiency) of load and speed, for each of the propulsive systems. The results of this further comparison are reported in Figures 19 and 20 for the two extreme cases ($T_4/T_1 = 3.5$; $\eta_T = 0.70$) and ($T_4/T_1 = 4.5$; $\eta_T = 0.75$), respectively. As is shown, the best efficiency curves of the compound system are always higher than the respective curves of the reference turbocharged engine, with efficiency improvement up to 10.9% in the first case (Figure 19) and up to 15.6% in the second case (Figure 20). Aiming to obtain an average evaluation of the benefit connected with the adoption of the compound system in a hybrid architecture vehicle, from Figures 19 and 20 it can be observed that the average efficiency increments, evaluated on the whole power range, are 6.1% in the case of $T_4/T_1 = 3.5$ and $\eta_T = 0.70$ and 11.2% in the case of $T_4/T_1 = 4.5$ and $\eta_T = 0.75$.

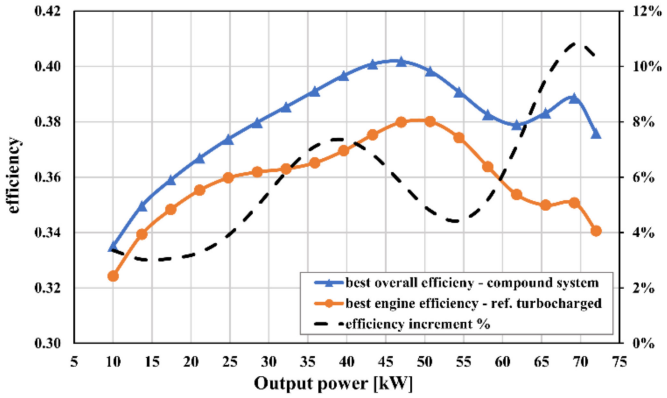

Figure 19. Comparison between the best efficiency curves of the compound engine with respect to the reference turbocharged engine (T_4/T_1 = 3.5 and η_T = 0.70).

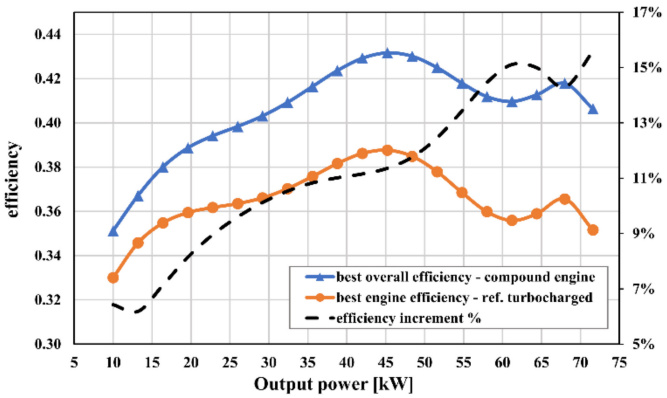

Figure 20. Comparison between the best efficiency curves of the compound engine with respect to the reference turbocharged engine (T_4/T_1 = 4.5 and η_T = 0.75).

According to the result obtained by this comparison, it can be concluded that the compound system revealed good potential for fuel economy improvement and related emission savings in hybrid vehicles, and that it is worth the effort related to further and deeper investigations. The priority for future developments is certainly the turbine generator design, whose performance greatly influences the advantages obtainable from the whole compound system. In addition, further studies should concentrate on the optimization of thermal–electric machine interactions in order to obtain the maximum energetic advantage from the whole hybrid system.

5. Conclusions

This paper deals with the energetic advantages related to the adoption of a separated electric turbo-compound propulsion unit for CNG-powered hybrid vehicles. The proposed compound system is composed of a supercharged CNG-fueled spark ignition engine equipped with an exhaust gas turbine generator dedicated to the unexpanded gas energy recovery. The supercharger is powered by an electric motor only when necessary (i.e., for manifold pressure higher than 1 bar), while the turbine generator is always active, continuously recovering energy from the whole exhaust gas mass flow. The system is particularly suitable for electric hybrid vehicle architectures in which the electric energy produced by the turbine generator can be stored on the vehicle storage system and hence profitably employed for vehicle propulsion.

The benefits connected to the implementation of the compound unit were evaluated with respect to a traditional CNG-fueled turbocharged reference engine, from the perspective of hybrid applications; for this purpose, a simple model was implemented by the authors, mainly based on power and mass flow balances, sometimes integrated by

experimental data. With the aim being to perform a fair and reasonable comparison, both the compound engine and the turbocharged reference engine were calculated starting from the same baseline naturally aspirated CNG engine. As described in the paper, the results obtained are influenced by a characteristic temperature ratio (T_4/T_1)—that is the ratio between the in-cylinder gas temperature when the exhaust valve opens (T_4) and the in-cylinder gas temperature when the inlet valve closes (T_1); this temperature ratio plays an important role, since it directly influences the temperature of the gas entering the turbine of both the turbocharged engine and the compound engine: it mainly depends on the particular engine and on the operating condition, and may assume values between 3.5 and 4.5. In order to provide the results with a general validity, three different values of this temperature ratio were considered in this paper, namely 3.5, 4.0 and 4.5. As also explained in the paper, the turbine considered for the compound engine substantially differs from common turbines employed for turbocharging purposes, with regards to both the high pressure ratios and the quasi steady operating conditions that characterize its application: for these reasons, with the aim being to ascertain the significance of the turbine efficiency in the compound engine performances, two plausible values were considered, i.e., $\eta_T = 0.70$ and $\eta_T = 0.75$. The effect of the exhaust back pressure increment on both the compound engine volumetric efficiency and the indicated efficiency was also taken into account: for each operating condition of the compound engine, the optimal exhaust pressure was hence determined by maximizing the compound system's overall efficiency.

Compared to the turbocharged reference engine, the compound propulsion unit revealed a lower brake specific fuel consumption, with a reduction of between 6.33% and 12.32%, depending on the temperature ratio T_4/T_1 and on the turbine efficiency η_T. The contribution of the turbine generator to the overall power produced by the compound system revealed maximum shares between 24.2% and 42.9%, with a maximum power output of between 15.2 and 23.3 kW: these results confirm that, if adequately recovered, the unexpanded exhaust gas energy may constitute a relevant part of the whole propulsion energy, and may significantly contribute to lowering both the vehicle fuel consumption and related emissions.

Considering the application to hybrid vehicles, a second comparison was carried out on an equal output power basis: the separated electric compound engine revealed efficiency increments, with respect to the reference turbocharged engine, of up to 12.5% when the lower efficiency turbine was assumed (i.e., $\eta_T = 0.70$), and up to 15.5% with the higher efficiency turbine (i.e., $\eta_T = 0.75$.), and, as discussed in the paper, the advantage associated with the exhaust gas energy recovery grows with the engine output power.

Considering that in hybrid propulsion vehicles, the internal combustion engine is usually employed in operating conditions close to the best efficiency curve, the authors also carried out a further comparison based on the best efficiency curves of both the compound engine and the turbocharged engine. This last comparison revealed that the compound propulsion unit could allow average efficiency improvement (i.e., on the whole output power range) of between 6.1% and 11.2%, depending on the temperature ratio and the turbine efficiency, with maximum benefits of 15.6% in the best case ($T_4/T_1 = 4.5$; $\eta_T = 0.75$).

The best efficiency improvements were obtained in the high-load/speed engine regions, with temperatures at the turbine inlet between 800 and 1000 °C, and maximum exhaust back pressures between 3.4 and 4.4 bar: these are not common conditions for traditional turbines used for turbocharging, and hence a dedicated study would be necessary for the development of the turbine generator, which could be represented by a multi-stage radial-axial turbine. Given the sensitivity of the overall efficiency of the compound system to the temperature ratio T_4/T_1 and to the turbine efficiency η_T, it follows that the best results can only be reached through an optimized design of the entire separated electric turbo-compound engine.

Author Contributions: E.P. contributed to the conceptualization and supervision of the work, to editing and writing of the paper; S.C. contributed to the acquisition and analysis of data, to the interpretation of results, and drafted the paper. All authors have read and agreed to the published version of the manuscript.

Funding: The research was funded by Università degli Studi di Palermo.

Institutional Review Board Statement: Not applicable.

Informed Consent Statement: Not applicable.

Data Availability Statement: All data generated or analyzed during this study are included in this published article or are publicly available.

Conflicts of Interest: The authors declare no conflict of interest.

Abbreviations and Symbols

$BMEP$	Brake mean effective pressure [bar]
$BMEP_{max}$	Maximum BMEP [bar]
$BMEP_{TOT}$	Overall BMEP of the compound engine [bar]
$BSFC$	Brake specific fuel consumption [g/kWh]
$BSFC_{TOT}$	Overall BSFC of the compound engine [g/kWh]
$CMEP$	Compressor mean equivalent pressure
$c_{p,C}$	Specific heat at constant pressure of the air
$c_{p,S}$	Specific heat at constant pressure of burned gas
EVO	Exhaust valve open
$FMEP$	Friction mean effective pressure
GCR	Geometrical compression ratio
G_{COMP}	Air mass flow of the compound engine
G_S	Turbine gas mass flow (turbocharged engine)
G_T	Engine air mass flow (turbocharged engine)
$ICEV$	Internal combustion engine vehicle
$IMEP$	Indicated mean effective pressure
$IMEP_g$	Gross indicated mean effective pressure
IVC	Inlet valve closure
k_S	Isentropic coefficient of the exhaust gas
LHV	Lower heating value of the fuel
m_{air}	Fresh air charge mass
MAP	Manifold absolute pressure
MAP_{max}	Maximum MAP
p_C	Boosting pressure
P_{comp}	Power required by the compressor
$PMEP$	Pumping mean effective pressure
p_S	Engine exhaust pressure
p_{S0}	Exhaust pipe pressure
P_{tur}	Power produced by the turbine
$R_{CNG}{}'$	Specific gas constant of natural gas
RGF	Residual gas fraction
R_{INT}	Intercooler efficiency
$RMEP$	Recovery mean equivalent pressure
$R_S{}'$	Specific gas constant of exhaust gas or burned gas
T	Temperature
T_0	Air temperature in the intake manifold
T_1	In-cylinder gas temperature at IVC
T_4	In-cylinder gas temperature at EVO
T_S	Exhaust gas temperature
T_T	Air temperature at the intercooler outlet
T'_T	Air temperature at the compressor outlet
u	normalized mean piston speed = $u_m/u_{m,max}$
u_m	mean piston speed

$u_{m,max}$	maximum mean piston speed
V_A	Naturally aspirated engine displacement
V_{COMP}	Engine displacement in the compound unit
V_T	Turbocharged engine displacement
φ	relative MAP = MAP/MAP_{max}
α	Air-fuel ratio
α_{ST}	Stoichiometric air-fuel ratio
β_C	Compressor pressure ratio
β_S	Exhaust gas turbine pressure ratio
δ_A	Air density in the intake manifold
δ_{COMP}	Density of the compressed air in the intake manifold for the compound engine
δ_T	Density of the compressed air in the intake manifold for the turbocharged engine
ε	Number of revolutions per cycle
η_b	Brake thermal efficiency of the engine
$\eta_{b,max}$	Maximum brake thermal efficiency of the engine
$\eta_{b,TOT}$	Overall brake thermal efficiency of the compound engine
η_C	Compressor efficiency
η_{EM}	Electric motor efficiency
η_i	Indicated thermal efficiency of the engine
$\eta_{i,g}$	Gross indicated thermal efficiency of the engine
η_S	Turbine efficiency of the reference turbocharged engine
η_T	Turbine efficiency of the compound engine
λ	Relative air-fuel ratio
λ_V	Volumetric efficiency of the engine
$\lambda_{V,COMP}$	Volumetric efficiency of the compound engine
$\lambda_{V,T}$	Volumetric efficiency of the reference turbocharged engine
Subscripts	
0	Reference condition
c	Compression/compressed
g	Gross
S	Exhaust gas

Appendix A. Residual Gas Fraction (RGF) Evaluation

When engine inlet valves close (IVC), the mass entrapped in the cylinder represents the sum of the residual gas from the previous cycle (m_S) and of the fresh charge (m_0); the residual gas fraction (RGF), which represents the ratio between the residual gas mass and the total in-cylinder mass, is thus:

$$RGF = \frac{m_S}{m_{TOT}} = \frac{m_S}{m_0 + m_S} \tag{A1}$$

The fresh charge mass entrapped in the cylinder depends on the engine volumetric efficiency λ_V:

$$m_0 = \lambda_V \cdot \frac{MAP}{R'_0 \cdot T_0} \cdot V \tag{A2}$$

where T_0 and MAP are the temperature and pressure in the intake manifold, respectively, and V is the engine displacement. Assuming the residual gas mass as the amount of in-cylinder exhaust gas at the ideal end of the exhaust stroke (i.e., at the top dead center):

$$m_S = \frac{p_S}{R'_S \cdot T_R} \cdot \left(\frac{V}{\rho - 1}\right) \tag{A3}$$

where T_R and p_S represent the temperature and pressure of the in-cylinder residual gas, ρ is the engine compression ratio, and hence $V/(\rho - 1)$ is the in-cylinder volume at the top dead center. The residual gas temperature T_R, in line with the simple approach followed in

this paper, can be evaluated while neglecting the heat transfer with in-cylinder wall during the exhaust stroke, thus assuming an isentropic transformation:

$$T_R = T_4 \cdot \left(\frac{p_4}{p_S}\right)^{\frac{1-k_S}{k_S}} \quad \text{(A4)}$$

where p_4 and T_4 are the in-cylinder gas pressure and temperature, respectively, when the exhaust valves open (EVO). As mentioned, the experimental findings confirmed by data reported in the scientific literature [24,35] show that for a spark ignition engine, the ratio T_4/T_1 ranges from 3.5 to 4.5. The isentropic coefficient k_S should be evaluated as a function of the exhaust gas composition and temperature, as described above (from Equations (36)–(39)).

References

1. European Commission. *Roadmap to a Single European Transport Area—Towards a Competitive and Resource Efficient Transport System*; European Commission: Brussels, Belgium, 2011.
2. European Environment Agency. *Monitoring CO_2 Emissions from Passenger Cars and Vans in 2018*; European Environment Agency: Copenhagen, Denmark, 2018. [CrossRef]
3. Eurostat. *Energy, Transport and Environment Statistics—2020 Edition*; Eurostat: Luxembourg, 2020; Available online: https://ec.europa.eu/eurostat/web/products-statistical-books/-/ks-dk-20-001 (accessed on 14 December 2021). [CrossRef]
4. Aghaali, H.; Ångström, H.-E. A review of turbocompounding as a waste heat recovery system for internal combustion engines. *Renew. Sustain. Energy Rev.* **2015**, *49*, 813–824. [CrossRef]
5. Alshammari, M.; Alshammari, F.; Pesyridis, A. Electric Boosting and Energy Recovery Systems for Engine Downsizing. *Energies* **2019**, *12*, 4636. [CrossRef]
6. Pasini, G.; Lutzemberger, G.; Frigo, S.; Marelli, S.; Ceraolo, M.; Gentili, R.; Capobianco, M. Evaluation of an electric turbo compound system for SI engines: A numerical approach. *Appl. Energy* **2016**, *162*, 527–540. [CrossRef]
7. Arsie, I.; Cricchio, A.; Pianese, C.; Ricciardi, V.; De Cesare, M. Evaluation of CO_2 reduction in SI engines with Electric Turbo-Compound by dynamic powertrain modelling. *IFAC-Papers OnLine* **2015**, *48*, 93–100. [CrossRef]
8. Millo, F.; Mallamo, F.; Pautasso, E.; Mego, G.G. The Potential of Electric Exhaust Gas Turbocharging for HD Diesel Engines. SAE Technical Paper. 2006. Available online: https://www.sae.org/publications/technical-papers/content/2006-01-0437/ (accessed on 14 December 2021). [CrossRef]
9. Hopmann, U.; Algrain, M.C. Diesel Engine Electric Turbo Compound Technology. SAE Technical Paper. 2003. Available online: https://www.sae.org/publications/technical-papers/content/2003-01-2294/ (accessed on 14 December 2021). [CrossRef]
10. Noor, A.M.; Puteh, R.C.; Rajoo, S.; Basheer, U.M.; Sah, M.H.M.; Salleh, S.H.S. Simulation Study on Electric Turbo-Compound (ETC) for Thermal Energy Recovery in Turbocharged Internal Combustion Engine. *Appl. Mech. Mater.* **2015**, *799*, 895–901. [CrossRef]
11. Kant, M.; Romagnoli, A.; Bin Mamat, A.; Martinez-Botas, R.F. Heavy-duty engine electric turbocompounding. *Proc. Inst. Mech. Eng. Part D J. Automob. Eng.* **2015**, *229*, 457–472. [CrossRef]
12. Cipollone, R.; Di Battista, D.; Gualtieri, A. Turbo compound systems to recover energy in ICE. *Int. J. Eng. Innov. Technol.* **2013**, *3*, 249–257. Available online: https://www.ijeit.com/Vol%203/Issue%206/IJEIT1412201312_41.pdf (accessed on 14 December 2021).
13. Zhuge, W.; Huang, L.; Wei, W.; Zhang, Y.; He, Y. Optimization of an Electric Turbo Compounding System for Gasoline Engine Exhaust Energy Recovery. SAE Technical Paper. 2011. Available online: https://www.sae.org/publications/technical-papers/content/2011-01-0377/ (accessed on 14 December 2021). [CrossRef]
14. Ghosh, T.K.; Prelas, M.A. *Energy Resources and Systems*; Springer: Dordrecht, The Netherlands, 2009; p. 778. ISBN 978-90-481-8494-1. [CrossRef]
15. Zhao, Y.; Chen, J. Performance analysis and parametric optimum criteria of an irreversible Atkinson heat-engine. *Appl. Energy* **2006**, *83*, 789–800. [CrossRef]
16. Hou, S.-S. Comparison of performances of air standard Atkinson and Otto cycles with heat transfer considerations. *Energy Convers. Manag.* **2007**, *48*, 1683–1690. [CrossRef]
17. Zhao, J.; Xu, F. Finite-Time Thermodynamic Modeling and a Comparative Performance Analysis for Irreversible Otto, Miller and Atkinson Cycles. *Entropy* **2018**, *20*, 75. [CrossRef] [PubMed]
18. Miller, R.H. Supercharging and Internal Cooling Cycle for High Output. *Trans. ASME* **1947**, *69*, 453–457.
19. Kawamoto, N.; Naiki, K.; Kawai, T.; Shikida, T.; Tomatsuri, M. Development of New 1.8-Liter Engine for Hybrid Vehicles. SAE Technical Paper. 2009. Available online: https://www.sae.org/publications/technical-papers/content/PT-143/3/#page=79 (accessed on 14 December 2021). [CrossRef]
20. Wang, Y.; Lin, L.; Zeng, S.; Huang, J.; Roskilly, A.P.; He, Y.; Huang, X.; Li, S. Application of the Miller cycle to reduce NOx emissions from petrol engines. *Appl. Energy* **2008**, *85*, 463–474. [CrossRef]

21. Chris, M.; Abul Masrur, M. *Hybrid Electric Vehicles: Principles and Applications with Practical Perspectives*, 2nd ed.; San Diego State University: San Diego, CA, USA, 2017; ISBN 978-111-897-053-9.
22. Pipitone, E.; Caltabellotta, S. Steady State Performance of Spark Ignition Engine with Exhaust Energy Recovery. SAE Technical Paper. 2020. Available online: https://iris.unipa.it/handle/10447/511686 (accessed on 14 December 2021). [CrossRef]
23. Millo, F.; Mallamo, F.; Digiovanni, R.; Dominici, A.; Morel, T.; Okarmus, M. Improving misfire diagnostic through coupled engine/vehicle numerical simulation. *SAE Trans.* **2004**, *113*, 466–475. Available online: https://www.jstor.org/stable/44723523 (accessed on 14 December 2021).
24. Heywood, J.B. *Internal Combustion Engine Fundamentals*; McGraw-Hill, Inc.: Cambridge, MA, USA, 2018; ISBN 126-011-610-7.
25. Xu, R.; Saggese, C.; Lawson, R.; Movaghar, A.; Parise, T.; Shao, J.; Choudhary, R.; Park, J.-W.; Lu, T.; Hanson, R.K.; et al. A physics-based approach to modeling real-fuel combustion chemistry—VI. Predictive kinetic models of gasoline fuels. *Combust. Flame* **2020**, *220*, 475–487. [CrossRef]
26. AMG GAS, Local Natural Gas Supplier. Available online: http://www.amg.pa.it/ (accessed on 14 December 2021).
27. D'Ambrosio, S.; Spessa, E.; Vassallo, A.; Ferrera, M.; Peletto, C. Experimental Investigation of Fuel Consumption, Exhaust Emissions and Heat Release of a Small-Displacement Turbocharged CNG Engine. SAE Technical Paper. 2006. Available online: https://www.sae.org/publications/technical-papers/content/2006-01-0049/ (accessed on 14 December 2021). [CrossRef]
28. Genchi, G.; Pipitone, E. Octane Rating of Natural Gas-Gasoline Mixtures on CFR Engine. *SAE Int. J. Fuels Lubr.* **2014**, *7*, 1041–1049. [CrossRef]
29. NIST Chemistry WebBook. Available online: https://webbook.nist.gov/chemistry/ (accessed on 14 December 2021).
30. Michon, M.; Calverley, S.; Clark, R.; Howe, D.; Chambers, J.; Sykes, P.; Dickinson, P.; Clelland, M.; Johnstone, G.; Quinn, R.; et al. Modelling and Testing of a Turbo-generator System for Exhaust Gas Energy Recovery. In Proceedings of the 2007 IEEE Vehicle Power and Propulsion Conference, Arlington, TX, USA, 9–12 September 2007; pp. 544–550. [CrossRef]
31. Nonthakarn, P.; Ekpanyapong, M.; Nontakaew, U.; Bohez, E. Design and Optimization of an Integrated Turbo-Generator and Thermoelectric Generator for Vehicle Exhaust Electrical Energy Recovery. *Energies* **2019**, *12*, 3134. [CrossRef]
32. Haughton, A.; Dickinson, A. Development of an Exhaust Driven Turbine-Generator Integrated Gas Energy Recovery System (TIGERS®). SAE Technical Paper. 2014. Available online: https://www.sae.org/publications/technical-papers/content/2014-01-1873/ (accessed on 14 December 2021). [CrossRef]
33. Pipitone, E.; Beccari, S. Performances and Emissions Improvement of an S.I. Engine Fuelled by LPG/Gasoline Mixtures. SAE Technical Paper. 2010. Available online: https://www.sae.org/publications/technical-papers/content/2010-01-0615/ (accessed on 14 December 2021). [CrossRef]
34. Pipitone, E.; Beccari, A. A Study on the Use of Combustion Phase Indicators for MBT Spark Timing on a Bi-Fuel Engine. SAE Technical Paper. 2007. Available online: https://iris.unipa.it/handle/10447/27795 (accessed on 14 December 2021). [CrossRef]
35. Bohac, S.V.; Assanis, D.N. Effect of Exhaust Valve Timing on Gasoline Engine Performance and Hydrocarbon Emissions. SAE Technical Paper. 2004. Available online: https://www.jstor.org/stable/44740919 (accessed on 14 December 2021). [CrossRef]